



## Summertime pollution events in the Arctic and potential implications

M. G. Iziomon,<sup>1</sup> U. Lohmann,<sup>2</sup> and P. K. Quinn<sup>3</sup>

Received 15 May 2005; revised 7 February 2006; accepted 8 March 2006; published 21 June 2006.

[1] Arctic summertime aerosols are examined here on the basis of column integrated and surface aerosol measurements made at Barrow (North Slope of Alaska) between 1998 and 2003. Although the site generally exhibits low aerosol burden in the summer, events of high loadings occur 8 days per summer. During the pollution episodes, the potential source contribution function from Russia is dominant (being about 40%). The source locations in Russia are mainly situated in the central and eastern parts. South Asia, Europe and North America each contribute 6% to the observed high aerosol loading. Source locations in south Asia lie in northern China and northern Japan, while those in Europe lie mainly in northern U.K. and Estonia. The North American sources are situated in northern Canada and Alaska. Over the 6-year period,  $10 \pm 4$  days per summer season show elevated levels of surface aerosol absorption. The pollution events with the highest aerosol absorption appear to be associated with smoke from wild fires burning in northwest Canada. Diurnally averaged top of the atmosphere direct radiative forcing  $\Delta F^{TOA}$  (550 nm) at Barrow lie between  $-1.50 \text{ W m}^{-2}$  and  $1.19 \text{ W m}^{-2}$  in summer with an annual mean of  $-0.53 \pm 0.11 \text{ W m}^{-2}$ . Given low Arctic summertime surface albedo (<30%), a positive  $\Delta F^{TOA}$  results when the single scattering albedo is 0.85 or lower. Summertime direct surface radiative forcing (550 nm) ranges between  $-3.2 \text{ W m}^{-2}$  and  $-29 \text{ W m}^{-2}$  for observed cases of aerosol optical depth at the site.

**Citation:** Iziomon, M. G., U. Lohmann, and P. K. Quinn (2006), Summertime pollution events in the Arctic and potential implications, *J. Geophys. Res.*, *111*, D12206, doi:10.1029/2005JD006223.

### 1. Introduction

[2] The Arctic region holds some of the potential answers to key questions about global climate change [Leck *et al.*, 2004]. In view of the thinning of Arctic sea ice [Hansen and Nazarenko, 2004] and the rapidly growing utilization of the Arctic, there is an increased need for a better understanding of aerosol properties as well as aerosol interaction with radiation, clouds and sensitive ecosystems in Polar regions. While the Arctic is remote from continental pollution sources, numerous studies have revealed that the Arctic atmosphere is being dramatically impacted by long-range transport of Asian dust and midlatitude emissions (including fossil fuel combustion, smelting and industrial activities) from about January to May [e.g., Bodhaine *et al.*, 1981; Rahn and Heidam, 1981; Barrie, 1986; Bodhaine and Dutton, 1993; Shaw, 1995; Sirois and Barrie, 1999; Quinn *et al.*, 2002; Koch and Hansen, 2005]. The winter/spring Arctic pollution phenomenon, also known as Arctic haze [Shaw, 1995], is enhanced by inefficient pollutants dispersal,

slow removal rates and isentropic transport into the Arctic as low-pressure systems run up against quasi-stationary Siberian high [Barrie, 1986].

[3] In view of the seasonality of Arctic haze and the associated meteorological flow fields, past studies on Arctic pollution have focused mainly on the Arctic winter and spring seasons. Two issues of the *Atmospheric Environment* (vol. 15, 1981, and vol. 19, 1985) and one issue of the *Geophysical Research Letters* (vol. 11, 1984), among others, were devoted to the investigation of this phenomenon. Arctic haze is characterized by high sulfate mass (derived from anthropogenic emissions of  $\text{SO}_2$ ) and other components such as soot [Shaw and Khalil, 1989; Barrie and Hoff, 1985; Scheuer *et al.*, 2003; Koch and Hansen, 2005]. Harris and Kahl [1994] report that about 20% of their back trajectories, which span 1985 to 1992, indicate near surface transport from north central Russia to Barrow during the Arctic haze season. On the basis of measurements from the Tropospheric Ozone Production about the Spring Equinox (TOPSE) campaign (taken from February to May 2000) over the North American Arctic Basin, Scheuer *et al.* [2003] present the evolution of particulate sulfate vertical distribution. They observed that as the season progressed surface haze diminished, while high-altitude haze increased. It was projected that mixing ratios of sulfate will continue to decline at all altitudes into the summer as low-level clouds and wet deposition processes will become more pronounced in removing sulfate aerosols from the atmosphere.

<sup>1</sup>Department of Physics and Atmospheric Science, Dalhousie University, Halifax, Nova Scotia, Canada.

<sup>2</sup>Institute for Atmospheric and Climate Science, ETH Zurich, Zurich, Switzerland.

<sup>3</sup>NOAA Pacific Marine Environmental Laboratory, Seattle, Washington, USA.

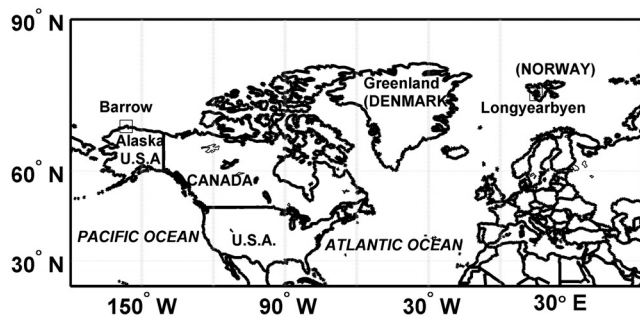


**Figure 1.** Map showing the study site at Barrow, North Slope of Alaska and surrounding regions.

[4] A long-term decrease in Arctic haze at Barrow has been reported by *Bodhaine and Dutton* [1993] on the basis of measurements of surface aerosol scattering and total column aerosol optical depth. The haze decrease was attributed to possible reduction in anthropogenic pollution emissions in Europe and the former Soviet Union [*Novakov et al.*, 2003]. *Polissar et al.* [1999] investigate the long-term trends and source locations for aerosols at Barrow using a three-way positive matrix factorization and a potential source contribution function. They report that industrial regions in Eurasia and North America are the major sources of high aerosol burden measured at Barrow in winter and spring. In summer, no major high potential source contribution function areas for black carbon and particles connected with light scattering were observed. Recently, *Koch and Hansen* [2005] used the Goddard Institute for Space Studies general circulation model to investigate the origins of Arctic black carbon, with main focus on Arctic Haze. The model suggests that predominant sources of Arctic soot today are from south Asia and from biomass burning (mostly from north of 40°N), being transported into the Arctic at high altitudes.

[5] The Arctic atmosphere is isolated effectively from lower latitudes by the polar front during summer. Open ice leads and ocean waters have been proposed as sources of Arctic aerosols during summer [*Ferek et al.*, 1995; *Polissar et al.*, 1999; *Leck et al.*, 2001]. *Quinn et al.* [2002] present a 3-year record of aerosol chemical and optical composition at Barrow. They report that sea salt, non-sea-salt (nss)  $\text{SO}_4^-$ ,  $\text{NH}_4^+$ , and the residual component dominate the aerosol mass. The remaining measured ionic species ( $\text{MSA}^-$ , nss  $\text{K}^+$ , nss  $\text{Mg}^{+2}$ , and nss  $\text{Ca}^{+2}$ ) contribute less than 10% and 4% to the aerosol submicron and supermicron mass, respectively. In particular, the residual mass in summer constitutes  $27.2 \pm 1.4\%$  of the supermicron aerosol mass and  $48.0 \pm 3.2\%$  of the submicron mass. The composition of this substantial summertime residual aerosol mass at Barrow is still presently unknown, although it is believed to be largely organics [*Quinn et al.*, 2002].

[6] While there is a wealth of knowledge about Arctic winter/spring atmospheric conditions, current understanding of summertime aerosol properties in the Arctic, as they relate to pollution, is still in its infancy. The magnitude and sign of radiative forcing by Arctic summertime aerosols as well as their environmental effects are still not well known [*Thomason et al.*, 2003]. Closely associated with this is the

paucity of reliable information on aerosol absorption [*Dubovik et al.*, 2002; *Kaufman et al.*, 2002], particularly over Arctic regions characterized by high surface albedo and harsh environmental conditions. The sparseness of such pertinent information leads to high uncertainty of aerosol optical properties in present aerosol radiation models and radiative forcing assessments [*Hansen et al.*, 1997; *Dubovik et al.*, 2002]. Furthermore, the role and occurrence of surface pollution in the Arctic (if any) during the summer are still uncertain. In this study, Arctic summertime aerosols are examined with particular emphasis on pollution events, their frequency and source regions. The meteorological summer season (i.e., June to August) is implied here. Surface and column integrated aerosol measurements obtained at Barrow (71.3°N, 156.6°W, 8 m a.s.l.), North Slope of Alaska (see Figure 1) are utilized. In addition to evaluating the distribution of summertime aerosol absorption at the Arctic site, this study investigates the potential effects of aerosol absorption on the sign and magnitude of the direct radiative forcing at the top of the atmosphere and at the surface.

## 2. Aerosol Measurements and Supplementary Data

[7] The National Oceanic and Atmospheric Administration (NOAA) commenced aerosol measurements at Barrow in 1976 [*Bodhaine et al.*, 1981]. With the aid of funding from the Atmospheric Radiation Measurement (ARM) Program, the aerosol sampling instrumentation was upgraded and expanded in October 1997. This study focuses on the measurements accruing from the newer instruments and sampling technique from 1998 to 2003. General details about the aerosol sampling system at Barrow have been presented in *Delene and Ogren* [2002] and *Quinn et al.* [2002]. In this section, only aerosol measurements that are related to this study are highlighted. Total aerosol light scattering coefficient ( $\sigma_s$ ) and hemispheric backscattering coefficient ( $\sigma_b$ ) for the aerosol aerodynamic diameter range of  $D < 1 \mu\text{m}$  and  $D < 10 \mu\text{m}$  are measured by a nephelometer at three wavelengths (450, 550 and 700 nm) and a low relative humidity ( $\leq 40\%$ ) over integration angles of  $\sim 7-170^\circ$  and  $90-170^\circ$ . These measurements were corrected to the full  $0-180^\circ$  and  $90-180^\circ$  ranges based on the Ångström exponent [*Anderson and Ogren*, 1998]. Aerosol light absorption coefficients  $\sigma_a$  for the same two size ranges are measured using a particle soot absorption photometer (PSAP) at  $\approx 550 \text{ nm}$ .

[8] The measurement uncertainties include errors due to noise, adjustment to standard temperature and pressure, calibration as well as adjustment to 550 nm for PSAP and correction for angular nonidealities for the nephelometer. These sources result in a total analytical uncertainty of about 10% in the measured nephelometer raw data [*Anderson and Ogren*, 1998; *Sheridan et al.*, 2001] and 15% in the PSAP [*Bond et al.*, 1999]. It is noteworthy that there are gaps in the aerosol data. These data gaps are either maintenance- or instrument-related [*Delene and Ogren*, 2002]. The aerosol hemispheric backscatter fraction  $b$  for the study period is derived from  $(\sigma_{b(550 \text{ nm})}/\sigma_{s(550 \text{ nm})})$ . The single scattering albedo  $\omega_0$  is given by  $(\sigma_{s(550 \text{ nm})}/(\sigma_{s(550 \text{ nm})} + \sigma_{a(550 \text{ nm})}))$  while the Ångström exponent  $\tilde{a}$  is obtained

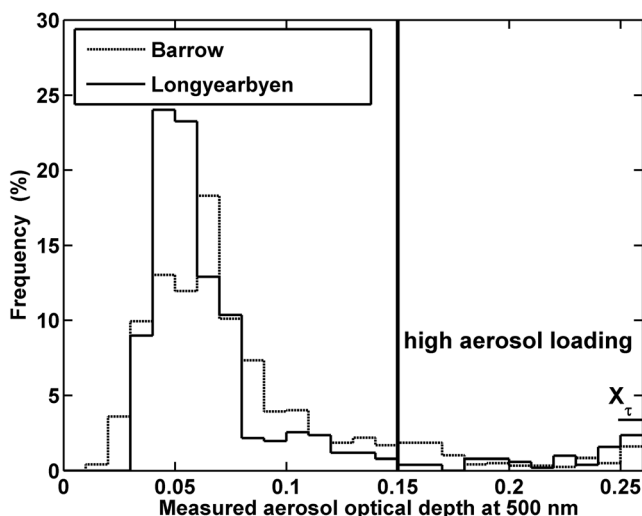


**Figure 2.** Composite frequency distribution of measured summertime aerosol optical depth (500 nm) at Barrow in 1999 and 2002. For comparison, the aerosol optical depth frequency distribution for another AERONET polar site, Longyearbyen, is also shown.

from  $(-\log[\sigma_s(450 \text{ nm})/\sigma_s(700 \text{ nm})]/\log(450/700))$  for the study period.

[9] An aerosol filter sampling system collects surface submicron and supermicron particles at the Arctic site for subsequent chemical analysis at the NOAA's Pacific Marine Environmental Laboratory (PMEL) [Quinn *et al.*, 2002]. Sample air is fed through a Berner-type multijet cascade impactor [Berner *et al.*, 1979] with aerodynamic cutoff diameters of 1 and 10  $\mu\text{m}$ . Aerosol particles with aerodynamic diameters ranging from 1 to 10  $\mu\text{m}$  are collected on a Tedlar film while those with diameters below 1  $\mu\text{m}$  pass through the impactor to a filter carousel housing 8 Millipore Fluoropore filters (1.0 pore size). The filters are weighed prior to and after the sampling procedures. The relative humidity of the sampled aerosol is less than 40%.

[10] The submicron filter samples are collected over a period of 1 to 5 days depending on the time of the year. A glove box (previously purged with air that has passed through a scrubber containing potassium carbonate and citric acid to get rid of  $\text{SO}_2$  and  $\text{NH}_3$ ) is used to handle all the filters and impactor films. At PMEL, the filters and films are wetted with 1 mL of spectral grade methanol. After adding 5 mLs of distilled deionized water to the solution, the substrates are extracted by sonicating for 30 min [Quinn *et al.*, 2001, 2002]. Since the glove box is kept at a constant humidity (33%), each sampled filter comes into equilibrium with the same vapor pressure of water thus minimizing experimental uncertainty due to a variable relative humidity [Quinn *et al.*, 2000]. After the final weighing, samples are analyzed by ion chromatography for major cations ( $\text{Na}^+$ ,  $\text{NH}_4^+$ ,  $\text{K}^+$ ,  $\text{Mg}^{2+}$ , and  $\text{Ca}^{2+}$ ) and anions ( $\text{Cl}^-$ ,  $\text{NO}_3^-$ ,  $\text{SO}_4^{2-}$  and  $\text{MSA}^-$ ) [Quinn *et al.*, 1998]. The concentration of nss  $\text{K}^+$ ,  $\text{Mg}^{+2}$  and  $\text{Ca}^{+2}$  were obtained from the measured value and the seawater ratio of the ion to  $\text{Na}^+$  assuming that all  $\text{Na}^+$  originated from sea salt [Quinn *et al.*, 2000]. More details about the

chemical analysis and measurement uncertainties are given by Quinn *et al.* [2002].

[11] NASA's AEROSOL ROBOTIC NETWORK (AERONET) Cimel sunphotometer is a multichannel automatic sun- and sky-scanning narrow field-of-view ground-based radiometer [Holben *et al.*, 2001]. The primary quantities measured by the Sun photometer include column-integrated aerosol optical depth  $\tau$  at predetermined discrete wavelengths (340, 380, 440, 500, 670, 870 and 1020 nm) and water vapor column abundance. The ground-based radiometer measurements are made during daylight (clear-sky) hours only. The aerosol particle size distribution is derived from the sky radiance measurements using radiative transfer algorithms [Dubovik *et al.*, 2000]. Aerosol optical thickness is derived to an accuracy of  $\pm 0.02$ – $0.04$  at an air mass of 2. For this study, level 2.0 quality-assured, cloud-screened AERONET data streams for Barrow are utilized. Broadband (280–2950 nm) shortwave downward and upward fluxes at the site are measured by ARM pyranometers at 1-min sampling intervals. This study utilizes broadband radiation data averaged hourly from 1998 to 2003.

### 3. Results and Discussion

#### 3.1. Pollution Episodes Inferred From Column-Integrated Aerosol Measurements

[12] Aerosol optical depth is the single most comprehensive variable to remotely assess the aerosol burden in the atmosphere [Holben *et al.*, 2001]. The short sampling interval of aerosols by AERONET photometer is particularly suited for responding to brief pollution episodes. While the time frame considered in this study extends from 1998 to 2003, AERONET aerosol optical depth measurements at Barrow are only available for 1999 and 2002 during this period. Consequently, Figure 2 presents the composite frequency distribution of instantaneous aerosol optical depth measurements at  $\lambda = 500 \text{ nm}$  during the summer of 1999 and 2002 at Barrow. Although the main focus of this study is Barrow, Figure 2 also presents the frequency distribution of  $\tau_{500}$  for another AERONET polar site, Longyearbyen ( $78^\circ\text{N}$ ,  $15^\circ\text{E}$ ), located in the Norwegian Arctic (see Figure 1). The data for the latter site are only available for 2003.

[13] As indicated in Figure 2, the bulk ( $\approx 60\%$  for Barrow and  $\approx 70\%$  for Longyearbyen) of the summertime aerosol optical depth data are less than 0.08, and are characteristic of Arctic background clean conditions [Shaw, 1982; Dutton *et al.*, 1984; Stone, 2001]. Of particular interest, however, are the observed cases of high summertime aerosol loadings ( $\tau_{500} \geq 0.15$ ). Aerosol levels of these magnitudes in the Arctic are indicative of pollution [Shaw, 1991]. Although uncommon in the summer, these elevated aerosol loadings occur with a frequency of 11% at Barrow and 9% at Longyearbyen in relation to the total observed clear sky events. Thus the occasional high aerosol optical depths observed at Barrow in summer are not only restricted to this Arctic location but seem to be characteristic of a larger area. Brock *et al.* [1989] observe haze particles (primarily sulfate and soot) above 850 mbar over Greenland and the North American Arctic in August 1985. Raatz and Shaw [1984] and Shaw [1985] report of pollution-derived metal residues and high proportion of sulfate in the Arctic air. The

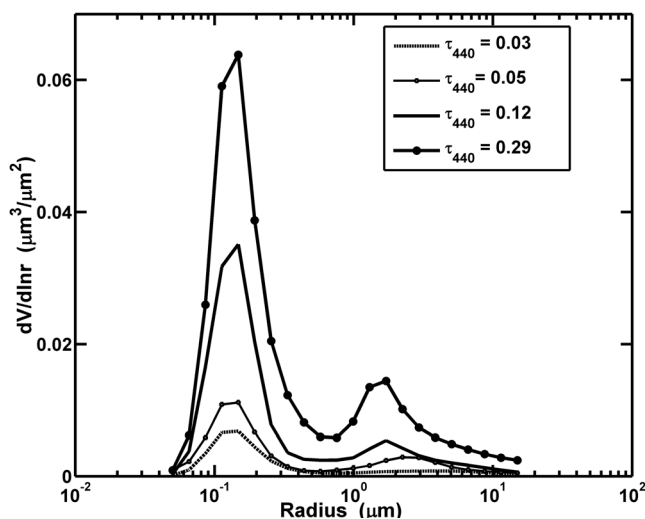


**Figure 3.** Mean summertime aerosol volume size for aerosol optical thickness  $\tau_{440}$  varying from 0.03 (clean condition) to 0.29 (polluted condition).

polar air mass (a lightly scavenged, dynamically stable system) teleconnects Alaska to pollution sources through general circulation [Shaw, 1991]. In what follows, these summertime pollution episodes at Barrow are further investigated on the basis of the suite of data available at this site.

[14] Figure 3 presents the mean summertime aerosol volume size for aerosol optical thickness (440 nm) varying from 0.03 (clean condition) to 0.29 (polluted condition) at Barrow. There is clearly a domination of accumulation mode aerosols. Relative to coarse aerosols, particles in the accumulation mode are most effective in reducing atmospheric transparency and therefore visibility. These sub-micron particles have the smallest dry deposition fluxes and wet removal rates. Consequently, they can travel hundreds to thousands of kilometers [Seinfeld and Pandis, 1998]. The long-range transport of atmospheric pollutants has major implications for the entire Arctic (and not just Barrow).

### 3.2. Potential Source Regions for Observed High Aerosol Loading

[15] Air mass trajectories from transport or dispersion models may be used to identify potential source regions for

aerosols. Cheng *et al.* [1993] and Hopke *et al.* [1995] used a conditional probability, defined as the potential source contribution function  $\rho$ , for identifying probable pathways and geographical source regions of biogenic, non-sea-salt sulfur observed in Alert Canada.  $\rho$  is inferred from trajectories arriving at the sampling site. It is given by [Polissar *et al.*, 1999]:

$$\rho_{ij} = P[B_{ij}|A_{ij}] = m_{ij}/n_{ij} \quad (1)$$

where  $P[A_{ij}]$  is a cumulative probability representing the potential for the transport of aerosols from a grid cell  $(i, j)$  to the receptor site,  $P[B_{ij}]$  denotes the probability that cell  $(i, j)$  is related to the observed high concentrations  $B_{ij}$ ,  $n_{ij}$  is the total number of trajectory endpoints that fall in the cell and  $m_{ij}$  represent the points for which a measured aerosol parameter exceeds a set criterion. Since  $\rho_{ij}$  is defined as the quotient of counts of selected events ( $m_{ij}$ ) and those of all events ( $n_{ij}$ ), it is impending that a small  $m_{ij}$  ( $\leq n_{ij}$ ) may result in  $\rho$  with high uncertainty in the high value [Polissar *et al.*, 1999]. To circumvent this drawback,  $\rho_{ij}$  is slightly modified such that  $m_{ij}$  relates to only pollution events sourced from a particular region, while  $n_{ij}$  is associated with all pollution events from all possible regions.  $\rho_{ij}$  becomes unity (i.e., 100%) when  $m_{ij} = n_{ij}$ .

[16] Here, the three-dimensional NOAA Air Resources Laboratory Hybrid Single Particle Lagrangian Integrated Trajectory (HYSPLIT4) model [Draxler and Hess, 1998] is utilized. Any given trajectory produced by this model is reasonably representative of the large-scale circulation, and as such may be used to suggest potential source regions [Polissar *et al.*, 1999]. It is noteworthy, however, that there are uncertainties in model trajectories regarding the exact path followed by an air parcel sampled at a particular location. Consequently, model trajectories should be considered as an indication of the general airflow rather than the exact pathway of an air parcel. In this study, the analyzed vertical wind fields from the National Centers for Environmental Prediction and the National Center for Atmospheric Research (NCEP/NCAR) reanalysis data were used to calculate the vertical transport of the air masses. The uncertainty of the HYSPLIT trajectory model ranges between 15% and 30% of the traveling distance [Pepler *et al.*, 2000].

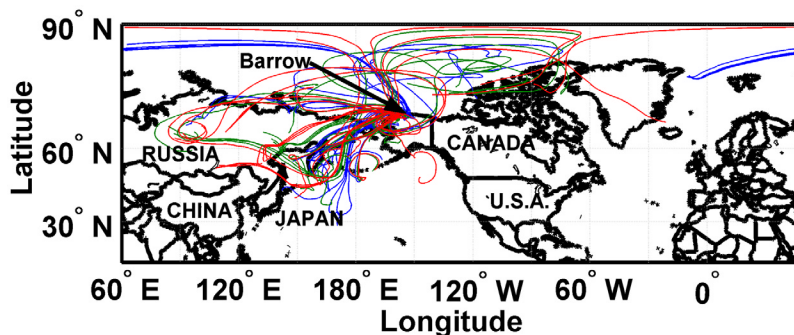


**Figure 4.** Eight-day HYSPLIT air mass back trajectories for three arrival heights (500 m, denoted by blue lines; 1000 m, denoted by green lines; and 1500 m, denoted by red lines) during the pollution episodes.

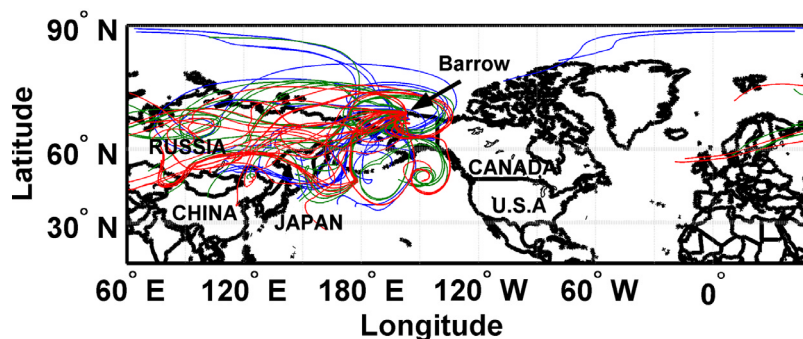


**Figure 5.** Same as Figure 4 but for high altitudes (2000 m, blue lines; 4000 m, green lines; and 6000 m, red lines).

[17] In relation to column-integrated aerosol optical depth, it is impossible to say a priori which transport altitudes are of utmost relevance. However, some studies on Arctic haze have indicated that the main altitude of transport is usually below 3 km [Shaw, 1991; Sharma *et al.*, 2004], with the pollution being most concentrated in the lowest 2 km of the atmosphere [Rahn and Heidam, 1981; Garrett *et al.*, 2004]. On the basis of their model study, Koch and Hansen [2005] have recently suggested that Asian pollution arrive in the Arctic at high altitude. In this study, two categories of transport levels are investigated. The first category (Class I) entails three low-level transport heights (500, 1000 and 1500 m above ground) while the second category (Class II) encompasses three high-level transport heights (2000, 4000 and 6000 m above ground). Days characterized by a series of instantaneous aerosol optical depth measurements with magnitude  $\approx 0.15$  and greater are classified as pollution days. Given this, 16 days (8 days each in 1999 and 2002) are clearly discernible as having recorded pollution events. The instantaneous aerosol optical depth data for the pollution days are averaged into hourly means and 8-day back trajectories for the observed pollution hours ( $\tau_{500} \geq 0.15$ ) are calculated. Periods with the same pollution source regions on a given pollution day are represented by one common trajectory. This method ensures that only trajectories that are representative of each pollution event are taken into consideration in the analysis.

[18] Typically, atmospheric aerosols have a tropospheric lifetime of about a week [Iziomon and Lohmann, 2003a]. Consequently, Figure 4 presents the calculated 8-day HYSPLIT back trajectories for Class I arrival heights at Barrow during the pollution event days, while Figure 5 presents the air mass back trajectories for Class II arrival heights. Rather than discuss the trajectory results based on specific locations, a regional zoning approach is adopted to facilitate comparison with earlier studies on Arctic haze. These regions include the Arctic Ocean (AO), northern Pacific Ocean, including Bering sea and sea of Okhotsk (PO), Russia (RS), south Asia (SA) and North America (NA). Back trajectories from Europe and the Atlantic are combined as EA. The potential source contribution function of the aforementioned regions at both low and high levels combined is presented in Figure 6. The source contributions for the individual levels are presented in Figure A1.

[19] For both low- and high-level heights, the potential source contribution function of Russia is dominant (being about 0.4 or 40% overall). The source locations in Russia are mainly situated in the central and eastern parts (namely Sakha, Khabarovsk Krai, Buryatia, Krasnoyarsky Krai, Evensky, Koryaksky, and Irkutskaya Oblast, see Figures 4 and 5). The foregoing is consistent with general circulation and chemical transport models, which have shown that Russia significantly affect lower-tropospheric air pollution in the Arctic particularly in winter and spring [Iversen, 1996]. Koch and Hansen [2005] report that during the Arctic Haze season, Russia contributes the most to Arctic sulfate optical thickness (24%). Thus summertime pollution episodes at Barrow are most frequently sourced by air masses from Russia.

[20] This is followed by transport over the Arctic Ocean and North Pacific Ocean, both of which show a potential source contribution function of 21% (overall). The Arctic

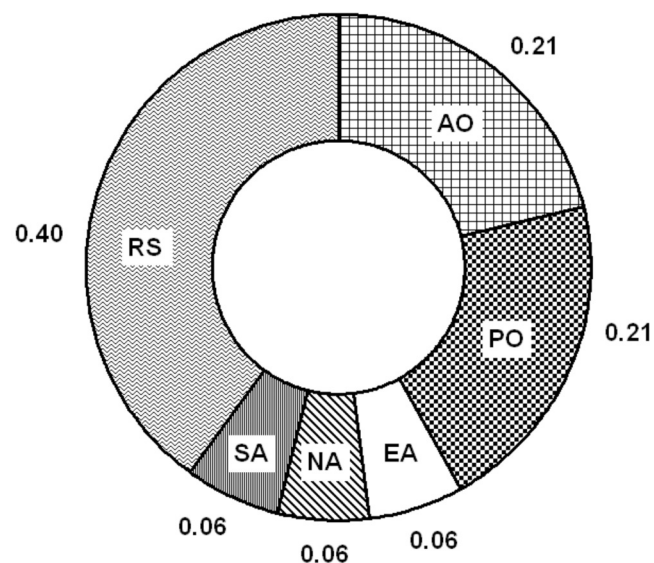


**Figure 6.** Overall potential source contribution functions to observed pollution episodes. While the Arctic Ocean (AO) and Pacific Ocean (PO) are not pollution sources in themselves, their air mass systems are capable of transporting pollution to the Arctic (see text). Russia, south Asia, Europe and North America are denoted by RS, SA, EA and NA, respectively.

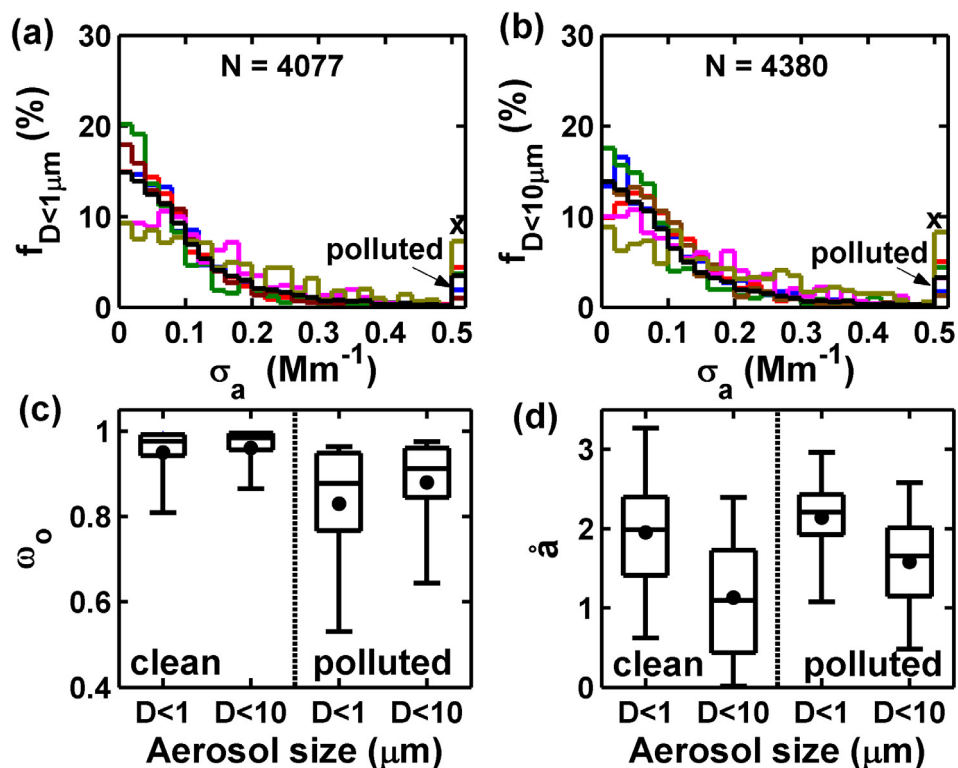


**Figure 7.** Summertime frequency distribution of hourly surface aerosol light absorption coefficients at Barrow from 1998 to 2003 for (a) submicron aerosols and (b) aerosols with  $D < 10 \mu\text{m}$ . The distributions for each individual year from 1998 to 2003 are depicted in blue, red, green, brown, violet, and dark yellow, respectively, while the overall distribution (for all the years combined) is shown in black. The region marked with a cross denotes  $\sigma_a > 0.5 \text{ Mm}^{-1}$ , and  $N$  is the sample size. (c) A plot of  $\omega_0$  and (d)  $\bar{a}$  for  $\sigma_a < 0.05 \text{ Mm}^{-1}$  (clean periods) and  $\sigma_a > 0.5 \text{ Mm}^{-1}$  (polluted periods) for submicron particles ( $D < 1 \mu\text{m}$ ) and the size range  $D < 10 \mu\text{m}$ . The bottom, middle and top horizontal lines in the boxes represent the 25th, 50th (median) and 75th percentile values, respectively, while the lower and upper error bars represent the 5th and 95th percentile values. The solid circles within the boxes denote mean values.

and North Pacific oceans are not pollution sources in themselves. However, their air mass systems are capable of transporting pollution to the Arctic. Shaw [1988, 1991] indicates that when the Arctic Ocean air mass system transports aerosols to the Arctic region, the composition of particles is characterized by pollution elements such as zinc and lead. The most likely route over which pollutants from eastern Asia could reach the Arctic is through the northern Pacific and the Bering Strait. Air carrying these aerosols would move eastward or northeastward across the Pacific Ocean in association with midlatitude westerlies, then cyclonically northward over the Bering Strait to the Arctic [Rahn, 1981; Barrie, 1986]. Harris and Kahl [1994] showed that during the Arctic haze season, over 30% frequency of transport originates from the North Pacific. South Asia, Europe and North America contribute much less (about 6% each) to the observed summertime episodes (Figure 6).

[21] Source locations in south Asia lie in northern China (Xinjiang, Inner Mongolia, Manchuria and Tianjin) and northern Japan (Asahikawa), while those in Europe lie mainly in northern U.K. and Estonia. The North American sources are mainly situated in northern Canada and Alaska. It is noteworthy that unlike the other source regions, the transport from south Asia (particularly China) mainly oc-

curred at high levels ( $\geq 4000 \text{ m}$ ) (see Figure 5). Harris and Kahl [1994] also report less frequent (10%) transport from Europe during Arctic Haze season. Although south Asia generates significant amount of pollutants such as  $\text{CO}$ ,  $\text{O}_3$  and hydrocarbons, some chemical modeling studies have shown that this region is not an important source region to the Arctic [Stohl *et al.*, 2002; Lamarque and Hess, 2003]. Absorbing pollutants at the surface are examined next.

### 3.3. Light Absorbing Aerosols

[22] Annually,  $\omega_0$  at Barrow reaches a maximum in the summer with a typical seasonal value of  $0.96 \pm 0.02$  [Quinn *et al.*, 2002; Delene and Ogren, 2002]. In this section, light-absorbing aerosol properties at the polar site are investigated with particular emphasis on pollution events. The summer mean values of  $\sigma_a$  are  $0.13 \pm 0.04 \text{ Mm}^{-1}$  for submicron particles and  $0.15 \pm 0.03 \text{ Mm}^{-1}$  for aerosols with  $D < 10 \mu\text{m}$  during the study period (1998–2003). Bodhaine [1995] presents aerosol absorption measurements at Barrow based on earlier Aethalometer record (1988–1993). The summer mean of  $\sigma_a$  observed here for submicron particles is in agreement with  $\approx 0.12 \text{ Mm}^{-1}$  reported by Bodhaine [1995].

[23] Figures 7a and 7b present the frequency distribution of hourly summer aerosol light absorption coefficients from 1998 to 2003 both for submicron particles and for particles

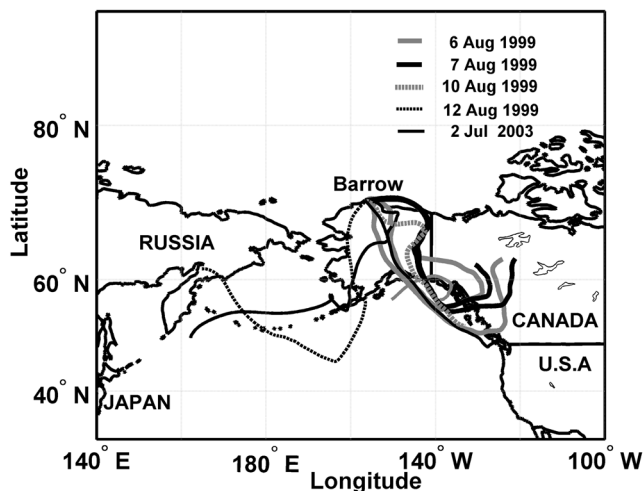


**Figure 8.** Eight-day HYSPLIT 500 m air mass back trajectories for days with the highest summertime light absorption coefficients at Barrow.

with  $D < 10 \mu\text{m}$  at Barrow. The left (i.e.,  $\sigma_a < 0.05 \text{ Mm}^{-1}$ ) and right tails (i.e.,  $\sigma_a > 0.5 \text{ Mm}^{-1}$ ) of the distribution are characteristic of clean and polluted episodes. Summertime light absorption coefficients beyond  $0.5 \text{ Mm}^{-1}$ , at the right end of the distribution, are more than three times the summer mean values stated previously. While such high summertime values of  $\sigma_a$  are rare in Barrow and are substantially less than those recorded at continental midwest

U.S. sites [Delene and Ogren, 2002], they are quite capable of producing significant optical effects at the remote site. The fact that there is no significant difference between the frequency distribution of  $\sigma_a$  for submicron particles and all measured aerosols shows that there is a preponderance of absorbing submicron particles in the aerosol distribution.

[24] Figures 7c and 7d present the single scattering albedo and Ångström exponent for  $\sigma_a < 0.05 \text{ Mm}^{-1}$  (clean air mass) and  $\sigma_a > 0.5 \text{ Mm}^{-1}$  (polluted air mass) for submicron particles and the full size range ( $D < 10 \mu\text{m}$ ). While  $\omega_0$  for aerosols with  $D < 10 \mu\text{m}$  averages  $0.88 \pm 0.02$  (uncertainties here represent the 95% confidence interval of the mean value) and  $0.96 \pm 0.003$  for polluted and clean periods respectively, the corresponding values are  $0.83 \pm 0.03$  and  $0.95 \pm 0.004$  for the submicron particles. Note that the mean values of  $\omega_0$  for the clean periods are close to those commonly reported in literature for summertime conditions in the Arctic [Quinn et al., 2002; Delene and Ogren, 2002]. Contrariwise, the pollution events result from aerosols of low  $\omega_0$ .

[25] The mean surface Ångström exponents for aerosols less than  $1 \mu\text{m}$  and those less than  $10 \mu\text{m}$  during the summer pollution episodes from 1998 to 2003 at Barrow are  $2.14 \pm 0.10$  and  $1.58 \pm 0.14$ , respectively. These aerosol size parameters are consistent with the Ångström exponents reported by Pepler et al. [2000] for pollutant absorbing aerosols. Over the 6-year summer period,  $10 \pm 4$  days per summer season (57 days in total) indicate pollution ( $\sigma_a > 0.5 \text{ Mm}^{-1}$ ) due to absorbing aerosols. This frequency range is consistent with that obtained in section 3.2. Figure 8 shows the 8-day back trajectories for days when

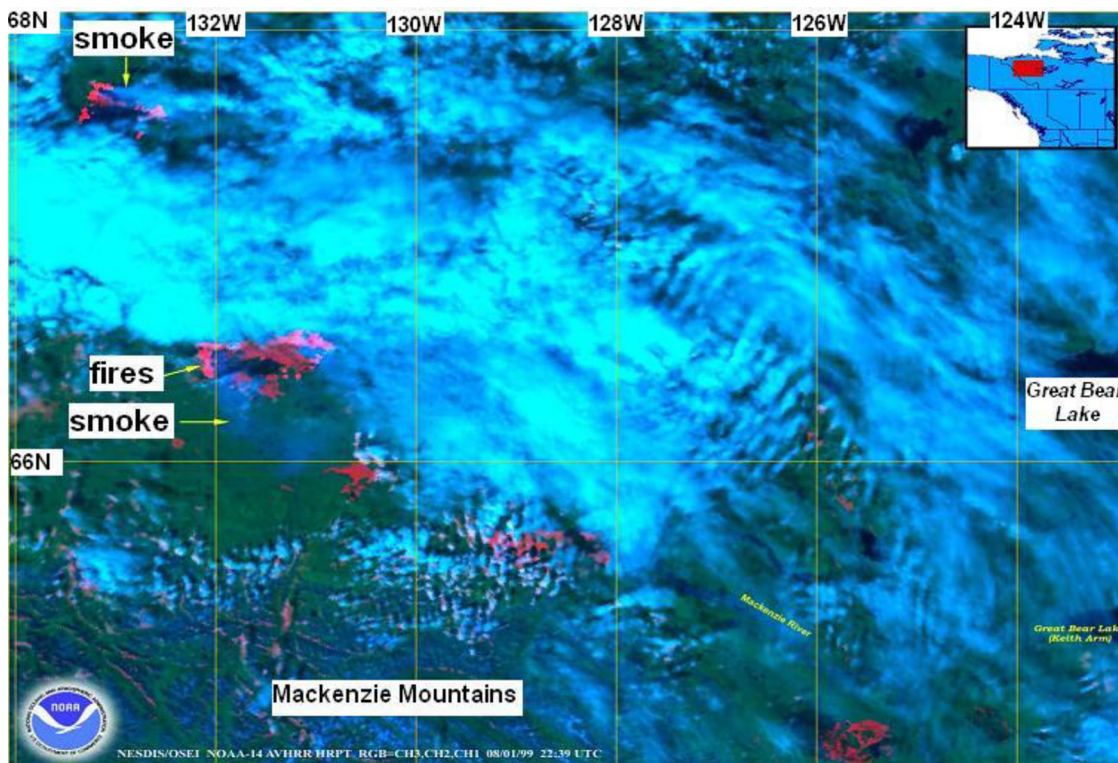


**Figure 9.** NOAA AVHRR image for 2239 UTC on 1 August 1999 showing heat signatures (red) and smoke (blue) haze from large areas of fire burning west of Great Bear Lake in the North West Territories of Canada.

**Table 1.** Submicron Light Absorption Coefficient ( $\sigma_a$ ), and Aerosol Chemistry for Pollution Events at Barrow<sup>a</sup>

Event Date	Max $\sigma_a$ , Mm <sup>-1</sup>	Ratio of Polluted to Clean Conditions		
		K <sup>+</sup>	Mg <sup>+2</sup>	Ca <sup>+2</sup>
11 Jun 1998	0.56	<1.0	1.0	<1.0
12 Jun 1998	0.58	<1.0	1.0	<1.0
5 Jul 1998	0.63	1.8	1.5	1.8
17 Jul 1998	0.86	2.4	3.0	1.8
19 Jul 1998	1.16	2.4	3.0	1.8
20 Jul 1998	1.02	5.4	8.9	3.6
1 Jun 1999	0.68	1.8	0.5	<1.0
2 Jun 1999	0.85	1.8	0.5	<1.0
11 Jul 1999	0.62	<1.0	<1.0	<1.0
2 Aug 1999	1.11	2.4	3.0	<1.0
5 Aug 1999	0.81	2.4	3.0	<1.0
6 Aug 1999	2.94	12.0	19.3	<1.0
7 Aug 1999	1.60	12.0	19.3	<1.0
10 Aug 1999	4.62	3.6	1.5	<1.0
12 Aug 1999	2.35	3.6	1.5	<1.0
6 Jun 2000	0.99	<1.0	<1.0	4.5
7 Jun 2000	0.67	<1.0	<1.0	4.5
16 Jun 2000	0.74	1.2	1.0	9.0
19 Jun 2000	0.76	1.2	1.0	9.0
20 Jun 2000	0.54	<1.0	<1.0	2.7
25 Aug 2000	0.70	<1.0	<1.0	<1.0
16 Jul 2001	0.58	1.1	<1.0	5.7
23 Jul 2001	1.01	1.6	<1.0	<1.0
12 Aug 2001	0.51	<1.0	2.8	<1.0
31 Aug 2001	0.56	<1.0	<1.0	<1.0
8 Jun 2002	0.84	1.7	2.9	1.4
9 Jun 2002	0.65	1.7	2.9	1.4
10 Jun 2002	0.53	1.7	2.9	1.4

<sup>a</sup>Only pollution days with aerosol chemistry data are presented here.

the highest summertime values of  $\sigma_a$  are recorded. The 500 m back trajectories, which are more relevant to surface level measurements [Pepler *et al.*, 2000; Quinn *et al.*, 2002], are presented. The air mass for these pollution periods originates mainly from northwest Canada and Russia. In line with these trajectories, NOAA AVHRR satellite images for late July and early August 1999 reveal several wild fires burning in northwest Canada. Figure 9 presents the image for 1 August 1999 showing smoke haze from large areas of fire burning west of Great Bear Lake in the North West Territories of Canada.

[26] Although the aerosol ionic chemical composition at Barrow is measured over longer timescale of about 5 days per segment, these data can serve as a valuable tool in determining the pollution sources when available. The approach here is to evaluate the ratio  $r_{pc}$  of the measured mass of submicron ionic aerosol components during pollution periods  $M_p$  to the average measured mass during clean periods  $\langle M_c \rangle$ . Thus, for a given aerosol component (i),

$$r_{pc}(i) = M_p(i) / \langle M_c(i) \rangle \quad (2)$$

[27] Submicron nss K<sup>+</sup> is a suitable tracer for biomass burning [Gaudichet *et al.*, 1995; Quinn *et al.*, 2002]. Subsequently, Table 1 presents the ratio  $r_{pc}$  for nss K<sup>+</sup> (used here as a tracer for biomass burning) during the pollution episodes. It is noteworthy that although a total of 57 summer days exhibit elevated levels of aerosol absorption during the 6-year period investigated here (see the preceding paragraph),

Table 1 only presents the pollution days when aerosol chemistry data are available at the site. In general,  $r_{pc}$  for K<sup>+</sup> ranges from 1.7 to 12 for 54% of the pollution episodes with chemistry data in Table 1.

[28] Dust aerosols are known to be partly absorbing at solar wavelengths [Seinfeld and Pandis, 1998]. This, however, is dependent on the source and size mode of the dust aerosols. Some studies conducted within the framework of the Asia Pacific Regional Aerosol Characterization Experiment (ACE-Asia) have reported single scattering albedo of  $\approx 0.96$  for dust aerosols [Doherty *et al.*, 2005]. Iziomon and Lohmann [2003b] and Clarke *et al.* [1996] report  $\omega_0$  for midlatitude and Safari dust aerosols as  $0.95 \pm 0.02$  and  $0.96-0.97$ , respectively. Malm *et al.* [1994] proposed the following equation for fine soil concentration after dividing by 0.86 to account for other compounds;

$$[\text{SOIL}] = 2.20[\text{Al}] + 2.49[\text{Si}] + 1.63[\text{Ca}] + 2.42[\text{Fe}] + 1.94[\text{Ti}] \quad (3)$$

However, since Al, Si, Fe and Ti are currently not measured at Barrow, Mg<sup>+2</sup> and Ca<sup>+2</sup> are used here as a tracer for soil dust [Malm *et al.*, 1994; Gong *et al.*, 2003; Zhang *et al.*, 2003]. It should be mentioned that these are soluble Mg and Ca, which are indicative of the presence of dust albeit not quantitatively. Thus, in addition to K<sup>+</sup>, Table 1 presents  $r_{pc}$  for nss Mg<sup>+2</sup> and Ca<sup>+2</sup> for pollution days when aerosol chemistry data are available. The ionic constituents Ca<sup>+2</sup> and Mg<sup>+2</sup> exhibit  $r_{pc} \geq 1.7$  during 36% and 39%, respectively, of the pollution periods. VanCuren and Cahill [2002] found that substantial levels of Asian dust are transported to North America at altitudes of 500–3000 m. The transport pathway to North America is understandably via the Pacific, where lofted Asian dust descends to the surface [Jaffe *et al.*, 1999; Wilkening *et al.*, 2000; Husar *et al.*, 2001]. It is observed that  $r_{pc}$  for Ca<sup>+2</sup> and Mg<sup>+2</sup> are high ( $\geq 1.7$ ) on some of the pollution days when  $r_{pc}$  for K<sup>+</sup> was considerable (i.e., about 2 or more). This could be suggestive of a possible mixture of dust and combustion aerosols as indicated by VanCuren [2003], who report that Asian dust is mixed with a substantial amount of combustion aerosols. Perry *et al.* [1999] also observe that black carbon is frequently mixed with dust over Hawaii in the springtime. The foregoing corroborates the presence of combustible and other absorbing aerosols at the Arctic site during summer. The radiative implications of this are discussed in the following two sections.

### 3.4. Top of the Atmosphere Direct Radiative Forcing

[29] Submicron aerosols have the greatest radiative impact on climate in the visible wavelengths. Consequently, radiative forcing is used as an indicator of potential climatic importance [Haywood and Shine, 1995]. The sign of the direct aerosol radiative forcing at the top of the atmosphere (TOA) is a function of the fraction of radiation scattered upward by aerosols  $\beta$ , the single scattering albedo and surface albedo  $\alpha$ . The boundary between cooling and heating by aerosols can be expressed relative to a critical single scattering albedo  $\omega_c$  [Seinfeld and Pandis, 1998] viz:

$$\omega_c = 2\alpha / [\beta(1 - \alpha)^2 + 2\alpha] \quad (4)$$

**Table 2.** Mean and Standard Error of Hourly Summertime Radiative Forcing Index  $\Delta\omega$  at Barrow as a Function of Measured Surface Albedo for Absorbing Aerosols  $\Delta\omega_{\text{abs}}$  ( $\omega_o < 0.88$ ) and Scattering Aerosols  $\Delta\omega_{\text{sca}}$  ( $\omega_o > 0.95$ ) From 1998 to 2003<sup>a</sup>

Measured Surface Albedo, %	$N_{\alpha}$ , %	$\Delta\omega_{\text{abs}}$	$\Delta\omega_{\text{sca}}$	$\Delta\omega_{\text{abs}} - \Delta\omega_{\text{sca}}$
$\alpha < 25$	74	$0.15 \pm 0.045$	$0.49 \pm 0.016$	-0.34
$25 < \alpha < 50$	10	$-0.034 \pm 0.047$	$0.24 \pm 0.031$	-0.27
$50 < \alpha < 75$	11	$-0.21 \pm 0.012$	$0.046 \pm 0.032$	-0.26
$75 < \alpha < 100$	5	$-0.21 \pm 0.010$	$-0.0053 \pm 0.0038$	-0.20

<sup>a</sup> $N_{\alpha}$  denotes the frequency of occurrence of observed surface albedo in the classified interval during the entire study period.

Aerosol impact is a warming if  $\Delta\omega < 0$  (where  $\Delta\omega = \omega_o - \omega_c$ ), but cooling otherwise. Table 2 presents the variation of  $\Delta\omega$  during the study period as a function of surface albedo for absorbing aerosols (with  $\omega_o(550 \text{ nm}) < 0.88$ ), which is typical of polluted Arctic air (see Figure 7) and scattering aerosols (with  $\omega_o(550 \text{ nm}) > 0.95$ ).  $\alpha$  is obtained from the ratio of measured downwelling and upwelling shortwave radiation at Barrow, and  $\beta$  at 550 nm is computed according to Anderson *et al.* [1999].

[30] Hourly averaged data of  $\alpha$  from 1998 to 2003 are grouped into four classes and the corresponding values of  $\Delta\omega$  are determined (see Table 2). Given any range of measured  $\alpha$ , light-absorbing aerosols exhibit lower  $\Delta\omega$  (denoted by  $\Delta\omega_{\text{abs}}$ ) relative to scattering aerosols ( $\Delta\omega_{\text{sca}}$ ).  $\Delta\omega_{\text{abs}} - \Delta\omega_{\text{sca}}$  ranges between -0.20 and -0.34. While scattering aerosols produce a net atmospheric cooling for  $\alpha < 75\%$ , absorbing aerosols exhibit a net warming for  $\alpha > 25\%$ . The latter is more pronounced at higher surface albedos  $\alpha > 50\%$  when the absorption of solar radiation by aerosols significantly exceeds the radiation scattered back to space. Next, the aerosol direct radiative forcing at the Arctic site is quantified.

[31] The top of the atmosphere (TOA) aerosol direct radiative forcing  $\Delta F^{\text{TOA}}$  [Charlson *et al.*, 1992; Chylek and Wong, 1995; Haywood and Shine, 1995] in visible wavelengths is given as:

$$\Delta F^{\text{TOA}} = -DS_o T_{\text{at}}^2 (1 - A_c) \omega_o \beta \tau \left\{ (1 - \alpha)^2 - (2\alpha/\beta)[(1/\omega_o) - 1] \right\} \quad (5)$$

where  $D$  is the fractional day length (i.e., the length of daytime given in parts of 24 hours),  $S_o$  is the solar constant ( $1370 \text{ W m}^{-2}$ ),  $T_{\text{at}}$  is the atmospheric transmission and  $A_c$  is the fractional cloud amount. The variables  $\alpha$ ,  $\omega_o(550 \text{ nm})$  and  $\beta(550 \text{ nm})$  are as previously defined. Aerosol optical depth at 550 nm is obtained by interpolation between 500 and 670 nm [Takemura *et al.*, 2002]. Although Haywood and Shine [1995] applied equation (5) for global mean conditions, here the shortwave  $\Delta F^{\text{TOA}}$  at 550 nm for Barrow is computed. It should be noted that (in contrast to  $\Delta\omega$ ) a positive  $\Delta F^{\text{TOA}}$  implies atmospheric warming and vice versa. The fractional day length at the Arctic site during the summer months is 1 [Bernhard *et al.*, 2003]. The average total cloud fraction at Barrow ranges from 0.77 and 0.86 in June and July, respectively, to 0.89 in August [Dong and Mace, 2003].  $T_{\text{at}}$  is deduced from the ratio of global solar radiation measured at the surface to incoming shortwave radiation at the top of the atmosphere [Van Meijgaard *et al.*,

2001]. As summertime aerosol optical depth measurements were mainly carried out during periods when the surface albedo is less than 30%, the  $\Delta F^{\text{TOA}}$  reported here should be considered as being for mainly snow-free conditions.

[32] Hourly (and diurnally averaged) top of the atmosphere direct radiative forcing at Barrow lie between  $-1.67 \text{ W m}^{-2}$  ( $-1.50 \text{ W m}^{-2}$ ) and  $+1.21 \text{ W m}^{-2}$  ( $+1.19 \text{ W m}^{-2}$ ) for a range of values of the variables in the two-stream radiative transfer approximation of equation (5), with a mean and standard error of  $-0.67 \pm 0.04 \text{ W m}^{-2}$  ( $-0.53 \pm 0.11 \text{ W m}^{-2}$ ). It should be emphasized that the results being presented here are for summer conditions only. The mean negative direct radiative forcing implies that aerosol cooling effect dominates. This is expected in view of the relatively low surface albedo values (see earlier discussion on  $\Delta\omega$ ). However, since the main concern here relates to the potential climatic impact of (absorbing) pollutant aerosols, Figure 10 presents the mean and standard error of shortwave direct radiative forcing as a function of single scattering albedo at Barrow. Observe the positive  $\Delta F^{\text{TOA}}$  (i.e., warming) for  $\omega_o \leq 0.85$  (absorbing aerosols) and the negative forcing for  $\omega_o > 0.85$  during snow-free conditions. In particular,  $\Delta F^{\text{TOA}}$  amounts to  $0.72 \pm 0.14 \text{ W m}^{-2}$  for  $\omega_o \leq 0.8$ . While this is comparable to the black carbon global mean TOA radiative forcing estimate of about  $0.5\text{--}0.8 \text{ W m}^{-2}$  [Haywood and Boucher, 2000; Jacobson, 2001], it constitutes only half of the direct radiative forcing reported by Valero *et al.* [1989] for the spring Arctic Haze season. As shown earlier, a warming aerosol effect is facilitated by a bright surface and low aerosol single scattering albedo. However, one remarkable feature of Figure 10 is that even with a low

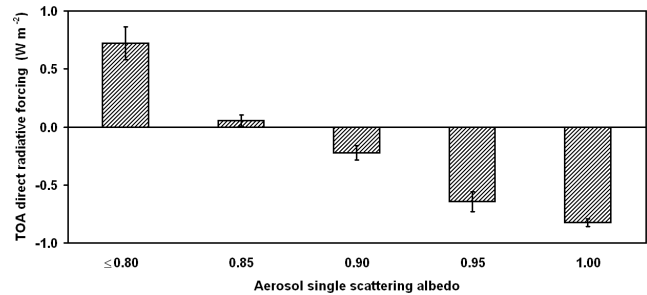


**Figure 10.** Mean direct radiative forcing (550 nm) at the top of the atmosphere (TOA) as a function of summertime aerosol single scattering albedo at Barrow. The first bin represents single scattering albedo less than (or equal to) 0.80, followed by those greater than 0.80 but less than (or equal to) 0.85 and so on.

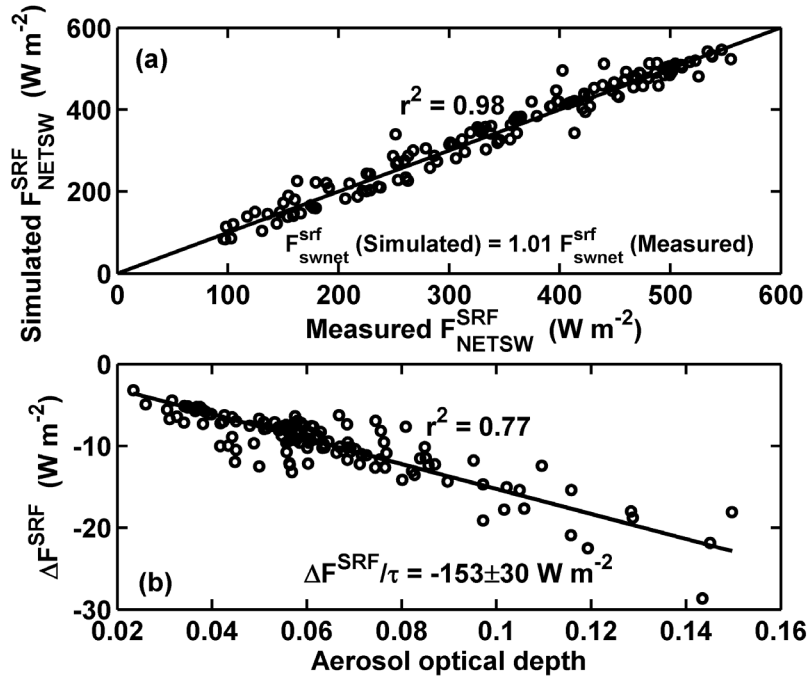


**Figure 11.** (a) Clear sky surface net shortwave flux at Barrow simulated using SBDART model versus ARM hourly averaged observations. (b) Surface direct radiative forcing (550 nm) at Barrow as a function of aerosol optical depth (550 nm).

surface albedo at Barrow in the summer, the TOA direct radiative forcing is positive given absorbing aerosols of  $\omega_o \leq 0.85$ . This highlights the potential radiative effect of pollutant absorbing aerosols.

### 3.5. Direct Surface Radiative Forcing

[33] The aerosol direct radiative forcing at the surface  $\Delta F^{SRF}$  represents the perturbation in the surface net flux due to aerosol presence in the atmospheric layers above [Hansell *et al.*, 2003]. Here,  $\Delta F^{SRF}$  is defined as the difference between the surface net shortwave flux with and without aerosols in the atmosphere:

$$\Delta F^{SRF} = F_{NETSW}^{SRF} - F_{NETSW}^{SRF(0)} \quad (6)$$

In equation (6),  $F_{NETSW}^{SRF}$  is the difference between the downwelling and upwelling shortwave flux with aerosols in the atmosphere and  $F_{NETSW}^{SRF(0)}$  is the corresponding aerosol-free net shortwave flux. Since there are no direct measurements of  $F_{NETSW}^{SRF(0)}$  at Barrow, it has to be computed from a radiative transfer model. This study utilizes the Santa Barbara Discrete Ordinate Radiative Transfer (DISORT) Atmospheric Radiative Transfer (SBDART) model [Ricchiuzzi *et al.*, 1998]. The plane-parallel radiative transfer equations are solved with the DISORT method [Stamnes *et al.*, 1988]. This model has been extensively used to study Arctic cloud radiative forcing [Intrieri *et al.*, 2002; Shupe and Intrieri, 2004]. The approach here is to first simulate hourly  $F_{NETSW}^{SRF}$  using the model and then compare these estimates to ARM measurements at Barrow.

[34] The model was run for all clear sky cases for which measured data of radiative fluxes and aerosol optical properties are available. Input variables for the model include standard atmospheric profile, measured column integrated

precipitable water, column ozone (obtained from NOAA CMDL Dobson spectrophotometer measurements for Barrow), surface albedo, Ångström exponent, aerosol optical depth, single scattering albedo and asymmetry parameter. The last three parameters are at 550 nm. Figure 11a presents the clear sky surface net shortwave flux at Barrow estimated using SBDART versus ARM measurements. There is a very good agreement between the simulated and measured  $F_{NETSW}^{SRF}$ , with both quantities agreeing within 7%. The mean bias between measured and simulated net shortwave flux is  $20 \text{ W m}^{-2}$ , which amounts to 3.6% of the measured maximum net shortwave flux. Thus the radiative transfer model is able to reproduce measured net shortwave flux at Barrow quite well.

[35]  $F_{NETSW}^{SRF(0)}$  at Barrow is then estimated from the model and  $\Delta F^{SRF}$  is obtained as given in equation (6). Figure 11b presents the surface direct radiative forcing (550 nm) at Barrow as a function of aerosol optical depth. Unlike  $\Delta F^{TOA}$  which could be positive or negative at Barrow,  $\Delta F^{SRF}$  is always negative, implying a cooling effect at the surface for both absorbing (pollutant) and scattering aerosols during summertime snow-free conditions. The surface radiative forcing increases linearly with aerosol loading, with values of  $\Delta F^{SRF}$  ranging from  $-3.2 \text{ W m}^{-2}$  to  $-29 \text{ W m}^{-2}$  for observed cases of aerosol optical depth.

[36] The rate at which the atmosphere is “forced” per unit optical depth (i.e.,  $\Delta F^{SRF}/\tau$ ) is known as the forcing efficiency [Anderson *et al.*, 1999]. It is given by the slope of Figure 11b and amounts to  $-153 \pm 30 \text{ W m}^{-2}$ . To the best of our knowledge, no summertime estimates of  $\Delta F^{SRF}/\tau$  for the Arctic are presently available other than the one reported here. However, the surface forcing efficiency at Barrow is much less than those found for industrial and urbanized regions. For instance, Hansell *et al.* [2003] report a surface

forcing efficiency of  $-286 \text{ W m}^{-2}$  for Asia while *Schafer et al.* [2002] report a forcing efficiency of  $-210 \text{ W m}^{-2}$  for the biomass region of south central Africa.

#### 4. Conclusion

[37] Current understanding of summertime aerosol properties in the Arctic as it relates to pollution is still in its infancy. In this study, summertime pollution events in the Alaskan Arctic are evaluated. Although the site generally records low aerosol burden (typical of Arctic background clean conditions) in the summer, events of high aerosol loadings do occur. These summertime elevated aerosol loadings occur with a frequency of 11% at Barrow and 9% at Longyearbyen (another AERONET polar site) in relation to the total observed clear sky events. Thus the occasional high aerosol optical depth observed at Barrow in summer are not only restricted to this Arctic location but seem to be characteristic of a larger area. There is clearly a domination of accumulation mode aerosols during the pollution events.

[38] Back trajectory analysis shows that the potential source contribution function of Russia is dominant (being about 40%) during the episodes. The source locations in Russia are mainly situated in the central and eastern part (namely Sakha, Khabarovsk Krai, Buryatia, Krasnoyarsk Krai, Evensky, Koryaksky, Irkutskaya Oblast). This supports past model studies, which have indicated that emissions and forest fires from Russia have a significant effect on lower-tropospheric air pollution in the Arctic [Iversen, 1996; Koch and Hansen, 2005]. South Asia, Europe and North America each contribute 6% to the observed high aerosol loading. Source locations in south Asia lie in northern China (Xinjiang, Inner Mongolia, Manchuria and Tianjin) and northern Japan (Asahikawa), while those in Europe lie mainly in northern U.K. and Estonia. The North American sources are mainly situated in northern Canada and Alaska. Unlike the other source regions, the transport from south Asia mainly occurred at high levels ( $\geq 4000 \text{ m}$ ).

[39] Over the 6-year period,  $10 \pm 4$  days per summer season show elevated levels of surface aerosol absorption coefficient ( $>0.5 \text{ Mm}^{-1}$ ). The events with the highest aerosol absorption appear to be associated with smoke from wild fires burning in northwest Canada. The ratio  $r_{pc}$  of the measured mass of submicron ionic aerosol components during pollution periods to the average measured mass during clean periods are evaluated. In general,  $\text{K}^+$  (used here as a tracer for soot) records high levels (with  $r_{pc}$  for  $\text{K}^+$  ranging from 1.7 to 12) during 54% of the pollution episodes while the ionic constituents  $\text{Ca}^{+2}$  and  $\text{Mg}^{+2}$  (used as a tracer for dust) exhibit  $r_{pc} \geq 1.7$  during 36% and 39%, respectively, of the pollution periods.

[40] Hourly (and diurnally averaged) estimates of clear sky top of the atmosphere direct radiative forcing  $\Delta F^{TOA}$  (550 nm) at the site range from  $-1.67 \text{ W m}^{-2}$  ( $-1.50 \text{ W m}^{-2}$ ) to  $1.21 \text{ W m}^{-2}$  ( $1.19 \text{ W m}^{-2}$ ) with a mean and standard error of  $-0.67 \pm 0.04 \text{ W m}^{-2}$  ( $-0.53 \pm 0.11 \text{ W m}^{-2}$ ). It is noteworthy that even with a low surface albedo in the summer, the direct radiative forcing is positive when  $\omega_0 \leq 0.85$ . This accentuates the potential impact of pollutant absorbing aerosols in the Arctic. The direct surface radiative forcing  $\Delta F^{SRF}$  (550 nm) at the site ranges between

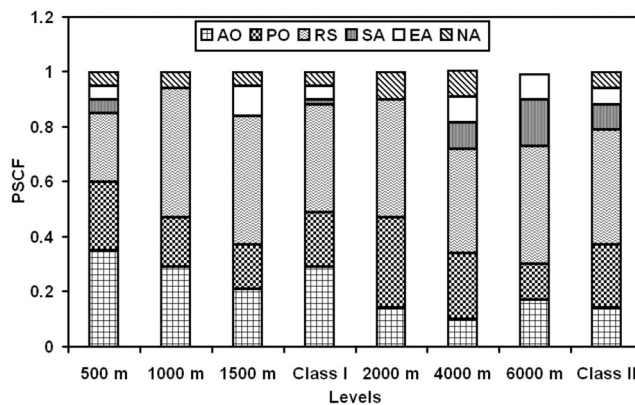


**Figure A1.** Low-level (500–1500 m) and high-level (2000–6000 m) potential source contribution functions (PSCF) to observed summer pollution events. Class I and II PSCFs represent the summary for the low and high levels respectively. The Arctic Ocean, Pacific Ocean, Russia, south Asia, Europe and North America are denoted by AO, PO, RS, SA, EA and NA, respectively.

$-3.2 \text{ W m}^{-2}$  and  $-29 \text{ W m}^{-2}$  for observed cases of aerosol optical depth, while the surface radiative forcing efficiency amounts to  $-153 \pm 30 \text{ W m}^{-2}$ .

[41] Relative to the Arctic haze season [Valero *et al.*, 1989] and in comparison to summertime conditions at continental Midwest U.S. locations [Delene and Ogren, 2002] or other urban centers [Hansell *et al.*, 2003], the Arctic summertime pollution reported here is of a much lesser magnitude. However, this study highlights their frequency of occurrence and potential radiative impacts. Additional data of aerosol optical properties and chemical composition at this polar site and other regions of the Arctic will go a long way to further enrich our understanding of Arctic summertime aerosols.

#### Appendix A

[42] As stated in section 3.2, the potential source contribution functions are estimated from the 8-day back trajectories arriving at Barrow. They identify probable source regions and likely transport pathways to the Arctic. The transport heights examined here ranges from 500 to 6000 m above ground. The potential source contribution functions to observed summer pollution events at each transport level are presented in Figure A1.

[43] **Acknowledgments.** The data used for this study were obtained from the Atmospheric Radiation Measurement Program sponsored by the U.S. Department of Energy, the NOAA Climate Monitoring and Diagnostics Laboratory, NOAA Air Resources Laboratory and NASA's AEROSOL ROBOTIC NETWORK. We thank John Ogren, Glen Lesins and the reviewers for helpful comments; Brent Holben for providing the AERONET data; and Paul Ricchiazzi, Shiren Yang and Catherine Gautier for providing the radiative transfer model. Moses Iziomon thanks the Canadian Foundation for Climate and Atmospheric Science and the Canadian Multiscale Air Quality Network for support.

#### References

Anderson, T. L., and J. A. Ogren (1998), Determining aerosol radiative properties using the TSI 3563 integrating nephelometer, *Aerosol Sci. Technol.*, 29, 57–69.

- Anderson, T. L., D. S. Covert, J. D. Wheeler, J. M. Harris, K. D. Perry, B. E. Trost, D. J. Jaffe, and J. A. Ogren (1999), Aerosol backscatter fraction and single scattering albedo: Measured values and uncertainties at a coastal station in the Pacific Northwest, *J. Geophys. Res.*, *104*, 26,793–26,807.
- Barrie, L. A. (1986), Arctic air pollution: An overview of current knowledge, *Atmos. Environ.*, *20*, 643–663.
- Barrie, L. A., and R. M. Hoff (1985), Five years of air chemistry observation in the Canadian Arctic, *Atmos. Environ.*, *19*, 1995–2010.
- Berner, A., C. Lurzer, F. Pohl, O. Preining, and P. Wagner (1979), The size distribution of the urban aerosol in Vienna, *Sci. Total Environ.*, *13*, 245–261.
- Bernhard, G., C. R. Booth, J. C. Ebrahimian, and V. V. Quang (2003), NSF polar programs UV spectroradiometer network 2000–2001 operations report, Biospherical Instruments Inc., San Diego, Calif.
- Bodhaine, B. A. (1995), Aerosol absorption measurements at Barrow, Mauna Loa, and the South Pole, *J. Geophys. Res.*, *100*, 8967–8975.
- Bodhaine, B. A., and E. G. Dutton (1993), A long term decrease in Arctic Haze at Barrow, Alaska, *Geophys. Res. Lett.*, *22*, 947–950.
- Bodhaine, B. A., J. M. Harris, and G. A. Herbert (1981), Aerosol light scattering and condensation nuclei measurements at Barrow, Alaska, *Atmos. Environ.*, *15*, 1375–1389.
- Bond, T. C., T. L. Anderson, and D. Campbell (1999), Calibration and intercomparison of filter-based measurements of visible light absorption by aerosols, *Aerosol Sci. Technol.*, *30*, 582–600.
- Brock, C. A., L. F. Radke, J. H. Lyons, and P. V. Hobbs (1989), Arctic hazes in summer over Greenland and the North American Arctic. I: Incidence and origins, *J. Atmos. Chem.*, *9*, 129–148.
- Charlson, R. J., S. E. Schwartz, J. M. Hales, R. D. Cess, J. A. Coakley Jr., J. E. Hansen, and D. J. Hofmann (1992), Climate forcing by anthropogenic aerosols, *Science*, *255*, 423–430.
- Cheng, M. D., P. K. Hopke, L. Barrie, A. Rippe, M. Olson, and S. Landsberger (1993), Qualitative determination of source regions of aerosol in Canadian High Arctic, *Environ. Sci. Technol.*, *27*, 2063–2071.
- Chylek, P., and J. Wong (1995), Effect of absorbing aerosols on global radiation budget, *Geophys. Res. Lett.*, *22*, 929–931.
- Clarke, A. D., J. N. Porter, F. Valero, and P. Pilewski (1996), Vertical profiles, aerosol microphysics, and optical closure during ASTEX: Measured and modeled column optical properties, *J. Geophys. Res.*, *101*, 4443–4453.
- Delene, D. J., and J. A. Ogren (2002), Variability of aerosol optical properties at four North American surface monitoring sites, *J. Atmos. Sci.*, *59*, 1135–1150.
- Doherty, S. J., P. K. Quinn, A. Jefferson, C. M. Carrico, T. L. Anderson, and D. Hegg (2005), A comparison and summary of aerosol optical properties as observed in situ from aircraft, ship, and land during ACE-Asia, *J. Geophys. Res.*, *110*, D04201, doi:10.1029/2004JD004964.
- Dong, X., and G. G. Mace (2003), Arctic stratus cloud properties and radiative forcing derived from ground-based data collected at Barrow, Alaska, *J. Clim.*, *16*, 445–461.
- Draxler, R. R., and G. D. Hess (1998), An overview of the HYSPLIT 4 modelling system for trajectories, dispersion and deposition, *Aust. Meteorol. Mag.*, *47*, 295–308.
- Dubovik, O., A. Smirnov, B. N. Holben, M. D. King, Y. J. Kaufman, T. F. Eck, and I. Slutsker (2000), Accuracy assessments of aerosol optical properties retrieved from AERONET sun and sky-radiance measurements, *J. Geophys. Res.*, *105*, 9791–9806.
- Dubovik, O., B. Holben, T. F. Eck, A. Smirnov, Y. J. Kaufman, M. D. King, D. Tanre, and I. Slutsker (2002), Variability of absorption and optical properties of key aerosol types observed in worldwide locations, *J. Atmos. Sci.*, *59*, 590–608.
- Dutton, E. G., J. J. DeLuise, and B. A. Bodhaine (1984), Features of aerosol optical depth observed at Barrow, March 10–20, 1983, *Geophys. Res. Lett.*, *11*, 385–388.
- Ferek, R. J., P. V. Hobbs, L. F. Radke, J. A. Herring, W. T. Sturges, and G. F. Cota (1995), Dimethyl sulfide in the arctic atmosphere, *J. Geophys. Res.*, *100*, 26,093–26,104.
- Garrett, T. J., C. Zhao, X. Dong, G. G. Mace, and P. V. Hobbs (2004), Effects of varying aerosol regimes on low-level Arctic stratus, *Geophys. Res. Lett.*, *31*, L17105, doi:10.1029/2004GL019928.
- Gaudichet, A., F. Echalar, B. Chatenet, J. P. Quisefit, G. Malingre, H. Cachier, P. Buat-Menard, P. Artaxo, and W. Maenhaut (1995), Trace elements in tropical African Savanna biomass burning aerosols, *J. Atmos. Chem.*, *22*, 19–39.
- Gong, S. L., X. Y. Zhang, T. L. Zhao, I. G. McKendry, D. A. Jaffe, and N. M. Lu (2003), Characterization of soil dust aerosol in China and its transport and distribution during 2001 ACE-Asia: 2. Model simulation and validation, *J. Geophys. Res.*, *108*(D9), 4262, doi:10.1029/2002JD002633.
- Hansell, R. A., S.-C. Tsay, Q. Ji, K. N. Liou, and S.-C. Ou (2003), Surface aerosol radiative forcing derived from collocated ground-based radiometric observations during PRIDE, SAFARI, and ACE-Asia, *Appl. Opt.*, *42*, 5533–5544.
- Hansen, J., and L. Nazarenko (2004), Soot climate forcing via snow and ice albedos, *Proc. Natl. Acad. Sci. U. S. A.*, *101*, 423–428.
- Hansen, J., M. Sato, and R. Ruedy (1997), Radiative forcing and climate response, *J. Geophys. Res.*, *102*, 6831–6864.
- Harris, J. M., and J. D. W. Kahl (1994), Analysis of 10-day isentropic flow patterns for Barrow, Alaska: 1985–1992, *J. Geophys. Res.*, *99*, 25,845–25,855.
- Haywood, J., and O. Boucher (2000), Estimates of the direct and indirect radiative forcing due to tropospheric aerosols: A review, *Rev. Geophys.*, *38*(4), 513–543.
- Haywood, J. M., and K. P. Shine (1995), The effect of anthropogenic sulfate and soot aerosol on the clear sky planetary radiation budget, *Geophys. Res. Lett.*, *22*, 603–606.
- Holben, B. N., et al. (2001), An emerging ground-based aerosol climatology: Aerosol optical depth from AERONET, *J. Geophys. Res.*, *106*, 12,067–12,097.
- Hopke, P. K., L. A. Barrie, S.-M. Li, M.-D. Cheng, C. Li, and Y. Xie (1995), Possible sources and preferred pathways for biogenic and non-sea-salt sulfur for the high Arctic, *J. Geophys. Res.*, *100*, 16,595–16,603.
- Husar, R. B., et al. (2001), Asian dust events of April 1998, *J. Geophys. Res.*, *106*, 18,317–18,330.
- Intrieri, J. M., C. W. Fairall, M. D. Shupe, P. O. G. Persson, E. L. Andreas, P. S. Guest, and R. E. Moritz (2002), An annual cycle of Arctic surface cloud forcing at SHEBA, *J. Geophys. Res.*, *107*(C10), 8039, doi:10.1029/2000JC000439.
- Iversen, T. (1996), Atmospheric transport pathways for the Arctic, in *Chemical Exchange Between the Atmosphere and Polar Snow*, *Global Environ. Change, NATO ASI Ser. I*, vol. 43, edited by E. Wolff and R. Bales, pp. 71–92, Springer, New York.
- Iziomon, M. G., and U. Lohmann (2003a), Optical and meteorological properties of smoke-dominated haze at the ARM Southern Great Plains Central Facility, *Geophys. Res. Lett.*, *30*(3), 1123, doi:10.1029/2002GL016606.
- Iziomon, M. G., and U. Lohmann (2003b), Characteristics and direct radiative effect of mid-latitude continental aerosols: The ARM case, *Atmos. Chem. Phys.*, *3*, 1903–1917.
- Jacobson, M. Z. (2001), Strong heating due to the mixing state of black carbon in atmospheric aerosols, *Nature*, *409*, 695–697.
- Jaffe, D. A., et al. (1999), Transport of Asian air pollution to North America, *Geophys. Res. Lett.*, *26*, 711–714.
- Kaufman, Y. J., J. V. Martins, L. A. Remer, M. R. Schoeberl, and M. A. Yamasoe (2002), Satellite retrieval of aerosol absorption over the oceans using sunglint, *Geophys. Res. Lett.*, *29*(19), 1928, doi:10.1029/2002GL015403.
- Koch, D., and J. Hansen (2005), Distant origins of Arctic black carbon: A Goddard Institute for Space Studies ModelE experiment, *J. Geophys. Res.*, *110*, D04204, doi:10.1029/2004JD005296.
- Lamarque, J.-F., and P. G. Hess (2003), Model analysis of the temporal and geographical origin of the CO distribution during the TOPSE campaign, *J. Geophys. Res.*, *108*(D4), 8354, doi:10.1029/2002JD002077.
- Leck, C., E. D. Nilsson, K. Bigg, and L. Bäcklin (2001), Atmospheric program on the Arctic Ocean Expedition 1996 (AOE-96): An overview of scientific goals, experimental approach, and instruments, *J. Geophys. Res.*, *106*, 32,051–32,067.
- Leck, C., M. Tjernström, P. Matrai, E. Swietlicki, and K. Bigg (2004), Can marine micro-organisms influence melting of the Arctic pack ice?, *Eos Trans. AGU*, *85*(3), 25.
- Malm, W. C., J. F. Sisler, D. Huffman, R. A. Eldred, and T. A. Cahill (1994), Spatial and seasonal trends in particle concentration and optical extinction in the United States, *J. Geophys. Res.*, *99*, 1347–1370.
- Novakov, T., V. Ramanathan, J. E. Hansen, T. W. Kirchstetter, M. Sato, J. E. Sinton, and J. A. Sathaye (2003), Large historical changes of fossil-fuel black carbon aerosols, *Geophys. Res. Lett.*, *30*(6), 1324, doi:10.1029/2002GL016345.
- Peppler, R. A., et al. (2000), ARM Southern Great Plains site observations of the smoke pall associated with the 1998 Central American fires, *Bull. Am. Meteorol. Soc.*, *81*, 2563–2591.
- Perry, K. D., T. A. Cahill, R. C. Schnell, and J. M. Harris (1999), Long-range transport of anthropogenic aerosols to the National Oceanic and Atmospheric Administration baseline station at Mauna Loa Observatory, Hawaii, *J. Geophys. Res.*, *104*, 18,521–18,533.
- Polissar, A. V., P. K. Hopke, P. Paatero, Y. J. Kaufmann, D. K. Hall, B. A. Bodhaine, E. G. Dutton, and J. M. Harris (1999), The aerosol at Barrow, Alaska: Long-term trends and source locations, *Atmos. Environ.*, *33*, 2441–2458.

- Quinn, P. K., D. J. Coffman, V. N. Kapustin, T. S. Bates, and D. S. Covert (1998), Aerosol optical properties in the marine boundary layer during the First Aerosol Characterization Experiment (ACE 1) and the underlying chemical and physical aerosol properties, *J. Geophys. Res.*, *103*, 16,547–16,564.
- Quinn, P. K., et al. (2000), Surface submicron aerosol chemical composition: What fraction is not sulfate?, *J. Geophys. Res.*, *105*, 6785–6805.
- Quinn, P. K., D. J. Coffman, T. S. Bates, T. L. Miller, J. E. Johnson, K. Voss, E. J. Welton, and C. Neusüss (2001), Dominant aerosol chemical components and their contribution to extinction during the Aerosols99 cruise across the Atlantic, *J. Geophys. Res.*, *106*, 20,783–20,810.
- Quinn, P. K., T. L. Miller, T. S. Bates, J. A. Ogren, E. Andrews, and G. E. Shaw (2002), A 3-year record of simultaneously measured aerosol chemical and optical properties at Barrow, Alaska, *J. Geophys. Res.*, *107*(D11), 4130, doi:10.1029/2001JD001248.
- Raatz, W. E., and G. E. Shaw (1984), Long-range tropospheric transport of pollution aerosols into the Alaskan Arctic, *J. Clim. Appl. Meteorol.*, *23*, 1052–1064.
- Rahn, K. A. (1981), Relative importances of North America and Eurasia as sources of Arctic aerosol, *Atmos. Environ.*, *15*, 1447–1455.
- Rahn, K. A., and N. Z. Heidam (1981), Progress in Arctic air chemistry, 1977–1980: A comparison of the first and second symposia, *Atmos. Environ.*, *15*, 1345–1348.
- Ricchiuzzi, P., S. Yang, C. Gautier, and D. Sowle (1998), SBDART: A research and teaching software tool for plane-parallel radiative transfer in the Earth's atmosphere, *Bull. Am. Meteorol. Soc.*, *79*, 2101–2114.
- Schafer, J. S., T. F. Eck, B. N. Holben, P. Artaxo, M. A. Yamasoe, and A. S. Procopio (2002), Observed reductions of total solar irradiance by biomass-burning aerosols in the Brazilian Amazon and Zambian Savanna, *Geophys. Res. Lett.*, *29*(17), 1823, doi:10.1029/2001GL014309.
- Scheuer, E., R. W. Talbot, J. E. Dibb, G. K. Seid, L. DeBell, and B. Lefer (2003), Seasonal distributions of fine aerosol sulfate in the North American Arctic basin during TOPSE, *J. Geophys. Res.*, *108*(D4), 8370, doi:10.1029/2001JD001364.
- Seinfeld, J. H., and S. N. Pandis (1998), *Atmospheric Chemistry and Physics*, 1326 pp., John Wiley, Hoboken, N. J.
- Sharma, S., D. Lavoué, H. Cachier, L. A. Barrie, and S. L. Gong (2004), Long-term trends of the black carbon concentrations in the Canadian Arctic, *J. Geophys. Res.*, *109*, D15203, doi:10.1029/2003JD004331.
- Shaw, G. E. (1982), Atmospheric turbidity in the polar regions, *J. Appl. Meteorol.*, *21*, 1080–1087.
- Shaw, G. E. (1985), Aerosol measurement in central Alaska, 1982–1984, *Atmos. Environ.*, *19*, 2025–2031.
- Shaw, G. E. (1988), Chemical air mass systems in Alaska, *Atmos. Environ.*, *22*, 2239–2248.
- Shaw, G. E. (1991), Aerosol chemical components in Alaska air masses: 1. Aged pollution, *J. Geophys. Res.*, *96*, 22,357–22,368.
- Shaw, G. E. (1995), The Arctic Haze phenomenon, *Bull. Am. Meteorol. Soc.*, *76*, 2403–2413.
- Shaw, G. E., and M. A. K. Khalil (1989), Arctic haze, in *The Handbook of Environmental Chemistry*, vol. 4, edited by O. Hutzinger, pp. 89–91, Springer, New York.
- Sheridan, P. J., D. J. Delene, and J. A. Ogren (2001), Four years of continuous aerosol measurement from the Department of Energy's Atmospheric radiation measurement program southern great plains cloud and radiation testbed site, *J. Geophys. Res.*, *106*, 20,735–20,747.
- Shupe, M. D., and J. M. Intrieri (2004), Cloud radiative forcing of the Arctic surface: The influence of cloud properties, surface albedo, and solar zenith angle, *J. Clim.*, *17*, 616–628.
- Sirois, A., and L. A. Barrie (1999), Arctic lower tropospheric aerosol trends and composition at Alert, Canada: 1980–1995, *J. Geophys. Res.*, *104*, 11,599–11,618.
- Stamnes, K., S. Tsay, W. Wiscombe, and K. Jayaweera (1988), Numerically stable algorithm for discrete-ordinate-method radiative transfer in multiple scattering and emitting layered media, *Appl. Opt.*, *27*, 2502–2509.
- Stohl, A., S. Eckhardt, C. Forster, P. James, and N. Spichtinger (2002), On the pathways and timescales of intercontinental air pollution transport, *J. Geophys. Res.*, *107*(D23), 4684, doi:10.1029/2001JD001396.
- Stone, R. S. (2001), Monitoring aerosol optical depth at Barrow, Alaska and South Pole; Historical overview, recent results and future goals, paper presented at 9th Workshop Italian Research on Antarctic Atmosphere, Soc. Ital. di Fis., Rome, Italy, 22–24 Oct.
- Takemura, T., T. Nakajima, O. Dubovik, B. N. Holben, and S. Kinne (2002), Single scattering albedo and radiative forcing of various aerosol species with a global three-dimension model, *J. Clim.*, *15*, 333–352.
- Thomason, L. W., A. B. Herber, T. Yamanouchi, and K. Sato (2003), Arctic Study on Tropospheric Aerosol and Radiation: Comparison of tropospheric aerosol extinction profiles measured by airborne photometer and SAGE II, *Geophys. Res. Lett.*, *30*(6), 1328, doi:10.1029/2002GL016453.
- Valero, F. P. J., T. P. Ackerman, and W. J. Y. Gore (1989), The effects of the arctic haze as determined from airborne radiometric measurements during AGASP II, *J. Atmos. Chem.*, *9*, 225–244.
- VanCuren, R. A. (2003), Asian aerosols in North America: Extracting the chemical composition and mass concentration of the Asian continental aerosol plume from long-term aerosol records in the western United States, *J. Geophys. Res.*, *108*(D20), 4623, doi:10.1029/2003JD003459.
- VanCuren, R. A., and T. A. Cahill (2002), Asian aerosols in North America: Frequency and concentration of fine dust, *J. Geophys. Res.*, *107*(D24), 4804, doi:10.1029/2002JD002204.
- Van Meijgaard, E., U. Andræ, and B. Rockel (2001), Comparison of model predicted cloud parameters and surface radiative fluxes with observations on the 100 km scale, *Meteorol. Atmos. Phys.*, *77*, 109–130.
- Wilkening, K. E., L. A. Barrie, and M. Engle (2000), Trans-Pacific air pollution, *Science*, *290*, 65–66.
- Zhang, X. Y., S. L. Gong, Z. X. Shen, F. M. Mei, X. X. Xi, L. C. Liu, Z. J. Zhou, D. Wang, Y. Q. Wang, and Y. Cheng (2003), Characterization of soil dust aerosol in China and its transport and distribution during 2001 ACE-Asia: 1. Network observations, *J. Geophys. Res.*, *108*(D9), 4261, doi:10.1029/2002JD002632.

M. G. Iziomon, Department of Physics and Atmospheric Science, Dalhousie University, Halifax, N. S., Canada B3H 4R2. (iziomon@mathstat.dal.ca)

U. Lohmann, Institute for Atmospheric and Climate Science, ETH Zurich, CH-8092 Zurich, Switzerland.

P. K. Quinn, NOAA Pacific Marine Environmental Laboratory, Seattle, WA 98115, USA.